LBNL-50069

ERNEST ORLANDO LAWRENCE
BERKELEY NATIONAL LABORATORY

Interpreting the Experimental Coexistence Curve of Finite Nuclear Matter

L. Phair, J.B. Elliott, L.G. Moretto,
and G.J. Wozniak

Nuclear Science Division

January 2002

Presented at the
International Winter Meeting on Nuclear Physics,
Bormio, Italy,
January 2002,
and to be published in
the Proceedings

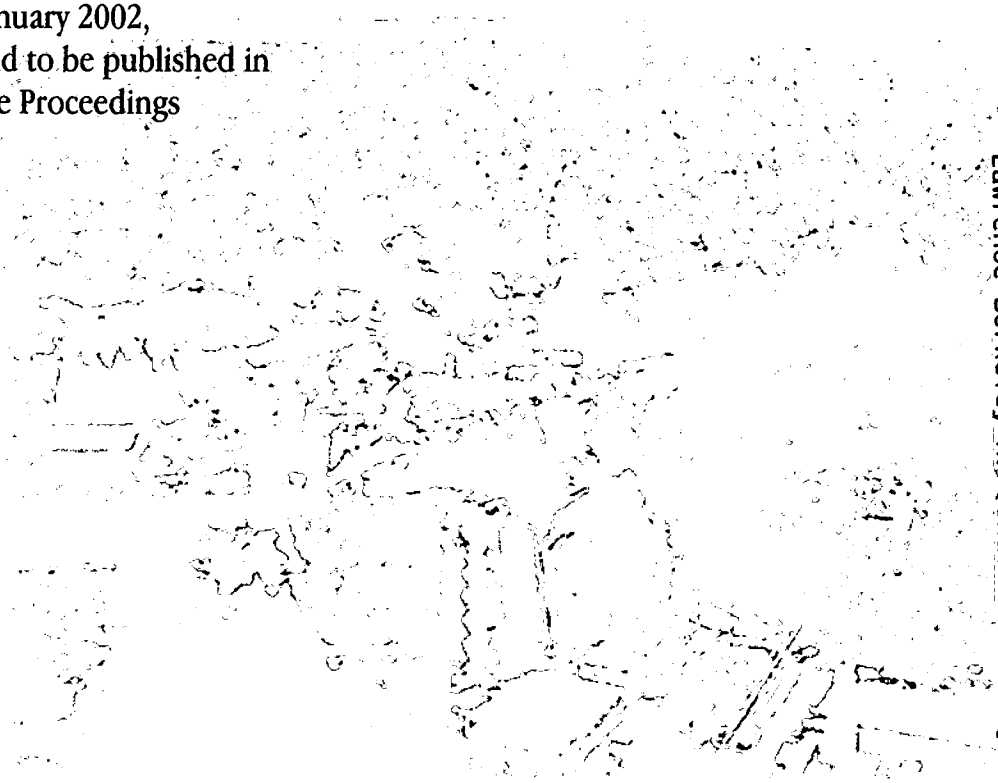

DISCLAIMER

LBNL-50069

Interpreting the Experimental Coexistence Curve of Finite Nuclear Matter

L. Phair, J.B. Elliott, L.G. Moretto, and G.J. Wozniak

Nuclear Science Division
Ernest Orlando Lawrence Berkeley National Laboratory
University of California
Berkeley, California 94720

January 2002

This work was supported by the Director, Office of Science, Office of High Energy and Nuclear Physics, Division of Nuclear Physics, of the U.S. Department of Energy under Contract No. DE-AC03-76SF00098.

Interpreting the Experimental Coexistence Curve of Finite Nuclear Matter

L. Phair*, J.B. Elliott*, L.G. Moretto* and G. J. Wozniak*

*Nuclear Science Division, Lawrence Berkeley National Laboratory, University of California, Berkeley, CA 94720

Abstract. The multifragmentation data of the ISiS Collaboration and the EOS Collaboration are examined. Fisher's droplet formalism, modi£ed to account for Coulomb energy, is used to determine the critical exponents τ and σ, the surface energy coef£cient c_0, the pressure-temperature-density coexistence curve of £nite nuclear matter, and the location of the critical point. Compound nucleus reactions are also described by the Fisher formalism when one considers the ensemble average of £rst-chance emission of rare particles. A pressure-temperature correlation can be inferred from the mean emission times (measured by the ISiS collaboration) which agrees very well with the pressure-temperature correlation inferred from the fragment yields.

INTRODUCTION

This work examines the formation of "fragments" from excited nuclei, termed "nuclear multifragmentation," which may be the result of a liquid-vapor phase transition [1, 2, 3]. Past analyses of nuclear multifragmentation have determined critical exponents [1, 4], examined caloric curves [5] and reported negative heat capacities [6]. More recent work has shown that three EOS experimental data sets [7] and the ISiS data set [8] contain a signature of a liquid-vapor phase transition manifested by the scaling behavior of Fisher's droplet formalism. Via Fisher's scaling, the coexistence line is observed over a large temperature interval extending up to and including the critical point. Critical exponents τ and σ, the critical temperature T_c, the surface energy coef£cient c_0, the compressibility factor C_F, the pressure-density-temperature coexistence curve, the critical pressure p_c and the critical density ρ_c can all be determined. This work considers the interpretation of these recently measured phase diagrams of nuclear matter [8].

THE DATA SETS

The Indiana Silicon Sphere (ISiS) Collaboration collected over $1,000,000$ events for the reaction 8.0 GeV/c $\pi+$ Au. For every event the fragment charge distribution was recorded for $1 \leq Z \leq 15$, fragments with $Z > 15$ were not elementally resolved [9]. Particles knocked out of the gold nucleus in the projectile-target collision were differentiated from the fragments formed from the excited remnant via a charge dependent kinetic energy cut [10]. An estimate was made of the charge of the fragmenting system Z_0 by subtracting the charge of the knockout particles from the charge of the gold nucleus. The mass of the fragmenting system A_0 was estimated by assuming that an average of 1.7 neutrons were knocked from the gold nucleus for every proton. The excitation energy per nucleon of the remnant E^* was constructed via energy balance considerations and the data was binned in terms of E^* in units of a tenth of an AMeV.

The EOS Collaboration collected $\approx 25,000$ fully reconstructed events ($76 \leq Z_{observed} \leq 82$) for the reaction 1.0 AGeV Au + C, $\approx 22,000$ fully reconstructed events ($54 \leq Z_{observed} \leq 60$) for 1.0 AGeV La + C, and $\approx$ 36,000 fully reconstructed events ($32 \leq Z_{observed} \leq 39$) for 1.0 AGeV Kr + C [11]. For every event, the charge and mass of the projectile remnant (Z_0, A_0) were determined by subtracting the charge and mass of the particles knocked out of the projectile from the charge and mass of the projectile. The knockout particles were distinguished from the fragments via a constant 30 MeV kinetic energy cut and E^*, constructed via energy balance considerations, was corrected for collective expansion effects [11]. The data for each system was binned in terms of E^* in units of half an AMeV.

ANALYSIS

The basis of the present analysis lies in an examination of the fragment yield distribution in the context of Fisher's droplet formalism [12]. Fisher gives the number of droplets of size A normalized to the size of the system as:

$$n_A(\varepsilon) = q_0 A^{-\tau} \exp\left(\frac{A\Delta\mu}{T} - \frac{c_0 \varepsilon A^{\sigma}}{T}\right), \quad (1)$$

where τ is the topological critical exponent (for three dimensions $2 \leq \tau \leq 3$); q_0 is a normalization constant depending solely on τ [13]; $\Delta\mu = \mu - \mu_{coex}$ with μ as the chemical potential of the system and μ_{coex} as the chemical potential at coexistence; T is the temperature; σ is a critical exponent related to the ratio of the dimensionality of the surface to the volume; c_0 is the zero temperature surface energy coeff£cient; $\varepsilon = (T_c - T)/T_c$ is a measure of the distance from the critical point; and T_c is the critical temperature. This form of the surface energy is applicable only for $T \leq T_c$.

Eq. (1) was modi£ed to account for the change in Coulomb energy (à la £ssion) when a fragment moves from the liquid to the vapor:

$$n_A = q_0 A^{-\tau} \exp\left(\frac{A\Delta\mu + E_{Coul}}{T} - \frac{c_0 \varepsilon A^{\sigma}}{T}\right), \quad (2)$$

where E_{Coul} is given by:

$$E_{Coul} = \frac{(Z_0 - Z)Z}{r_0\left((A_0 - A)^{1/3} + A^{1/3}\right)}\left(1 - e^{-x\varepsilon}\right). \quad (3)$$

Here $r_0 = 1.2$ fm. The term $1 - e^{-x\varepsilon}$ gives an account of the Coulomb energy behavior that vanishes as $x\varepsilon$ near T_c where no distinction exists between liquid and vapor. The fragment mass prior to decay was assumed to be

$$A = 2Z(1 + y(E^*/B_f)), \quad (4)$$

where B_f is the binding energy of the fragment and y is a £t parameter that allows for more or less decay. The temperature was determine via a degenerate Fermi gas, $T = \sqrt{E^*/\alpha}$, where $\alpha = 8(1 + (E^*/B_0))$ [14] to accommodate the empirically observed change in α with E^* [15]. B_0 is the binding energy of the fragmenting system. The total number of fragments N_A of size A was normalized to the size of the fragmenting system A_0, $n_A = N_A/A_0$.

RESULTS

For the ISiS data set, over 500 data points for $1.5 \leq E^* \leq 6.0$ AMeV and $5 \leq Z \leq 15$ were simultaneously £t to Eq. (2) with the parameters $\Delta\mu$, x, τ, σ, c_0 and T_c allowed to vary to minimize chi-squared. The secondary decay parameter was £xed at $y = 1$. Fragments with $Z < 5$ were not considered in the £t because Fisher's model expresses the mass/energy of a fragment in terms of bulk and surface energies and this approximation is known to fail for the lightest of nuclei where shell effects dominate. Also, for the lightest fragments equilibrium and non-equilibrium production cannot always be differentiated.

Table 1 gives the resulting £t values. The values of τ and σ are close to those expected for some three dimensional systems: $\tau \approx 2.2$ and $\sigma \approx 2/3$ and are in agreement with other multifragmentation results [16, 17]. The small positive $\Delta\mu$ value may indicate that the system is a supersaturated vapor. The value of c_0 is close to the value of the surface energy coeff£cient of the liquid-drop model, approximately 17 MeV. The value of T_c is close to theoretical estimates [18].

Figure 1 shows the results of this analysis. The fragment mass yields are scaled by the power law pre-factor, the bulk term and the Coulomb energy, $n_A/q_0A^{-\tau}\exp(\Delta\mu A + E_{Coul}/T)$, and are plotted against the temperature scaled by the surface energy, $A^{\sigma}\varepsilon/T$. The scaled data collapse to a single straight line over six orders of magnitude, precisely the behavior of a system undergoing a liquid-vapor transition [19]. This line is the liquid-vapor coexistence line and provides direct evidence of the liquid-vapor transition in excited nuclei.

For the EOS data sets, E_c^* (listed in Table 2) was determined by the peak of the RMS □uctuations of the charge of the largest fragment normalized to Z_0, as shown in Fig. 2. The values of E_c^* are close to previous observations in the EOS data [4, 11] and lead to T_c values that are comparable to theoretical estimates [18]. The topological exponent was £xed at $\tau = 2.2$ in keeping with the value for a variety of three dimensional systems [20] and myriad multifragmentation studies [1, 4]. There were 174 data points for 0.25 AMeV $\leq E^* \leq E_c^*$ and $5 \leq Z \leq Z_0/4$ from the three data sets simultaneously £t to Eq. (2). The parameters σ and c_0 were kept consistent between data sets while $\Delta\mu$, x and y were allowed to vary between them.

The results are recorded in Table 1. The exponent values are in the range expected in Fisher's formalism for some three dimensional systems and are in agreement with those previously determined for the EOS [4] and ISiS gold multifragmentation data [17, 8], as expected for critical phenomena [21]. The surface energy coeff£cient c_0 is close to the value of the surface energy coeff£cient of the liquid-drop model. The differences in E_c^* and T_c between the ISiS and EOS data are due to the differences in differentiation between knockout particles and fragments; this difference leads to ${}^{EOS}E^* \approx 1.2\,{}^{ISiS}E^*$ [10] which accounts for the differing results; this difference affects all energy related quantities, e.g. c_0. The

TABLE 1. Fit parameters

System	τ	σ	β	c_0 (MeV)	$\Delta\mu$ (AMeV)	x	y
ISiS π+ Au	2.18 ± 0.14	0.54 ± 0.01	0.33 ± 0.25	18.3 ± 0.5	0.06 ± 0.03	1.0 ± 0.06	1.00 (£xed)
EOS Au + C	2.2 (£xed)	0.69 ± 0.02	0.30 ± 0.01	14 ± 1	0.38 ± 0.02	1.0 ± 0.1	0.43 ± 0.06
EOS La + C	2.2 (£xed)	0.69 ± 0.02	0.30 ± 0.01	14 ± 1	0.42 ± 0.03	1.2 ± 0.1	0.33 ± 0.08
EOS Kr + C	2.2 (£xed)	0.69 ± 0.02	0.30 ± 0.01	14 ± 1	0.61 ± 0.05	3.9 ± 0.7	0.70 ± 0.20

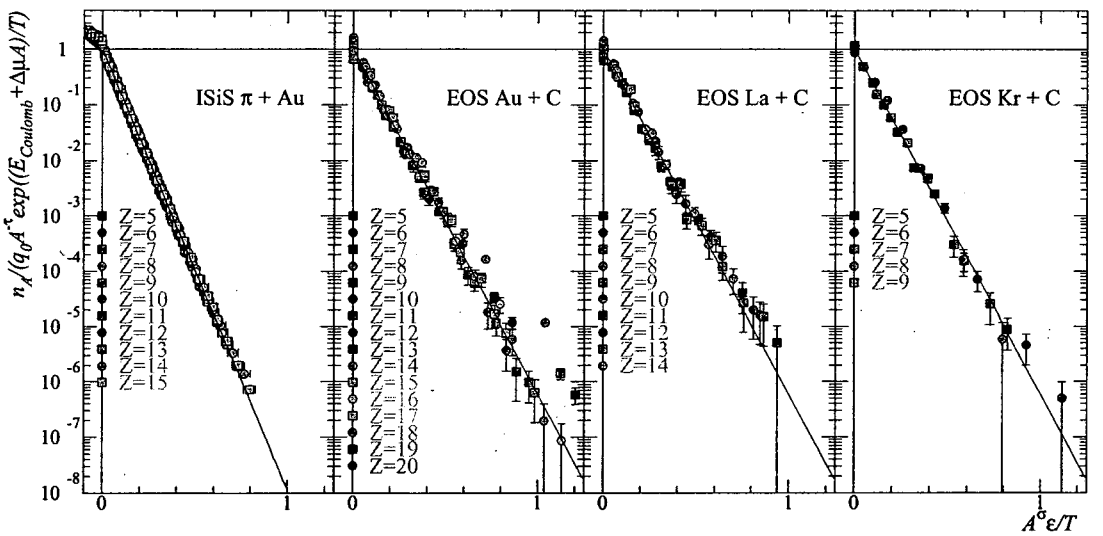

FIGURE 1. Left to right: The scaled fragment distributions of the ISiS gold data, the EOS gold, lanthanum and krypton data.

TABLE 2. Thermodynamic properties of excited nuclei

System	E_c^* (AMeV)	T_c (MeV)	ρ_c (ρ_0)	p_c (MeV/fm^3)	ΔH (MeV)	ΔE (AMeV)	C_c^F
ISiS π+ Au	3.8 ± 0.3	6.7 ± 0.2	~ 0.3	~ 0.07	26 ± 1	~ 15	0.25 ± 0.06
EOS Au + C	4.75 ± 0.25	7.7 ± 0.2	~ 0.36	~ 0.11	20.0 ± 0.9	~ 11	0.3 ± 0.1
EOS La + C	4.75 ± 0.25	7.7 ± 0.2	~ 0.36	~ 0.11	20.0 ± 0.9	~ 11	0.3 ± 0.1
EOS Kr + C	5.25 ± 0.25	8.2 ± 0.2	~ 0.37	~ 0.13	21.0 ± 1.0	~ 11	0.3 ± 0.1

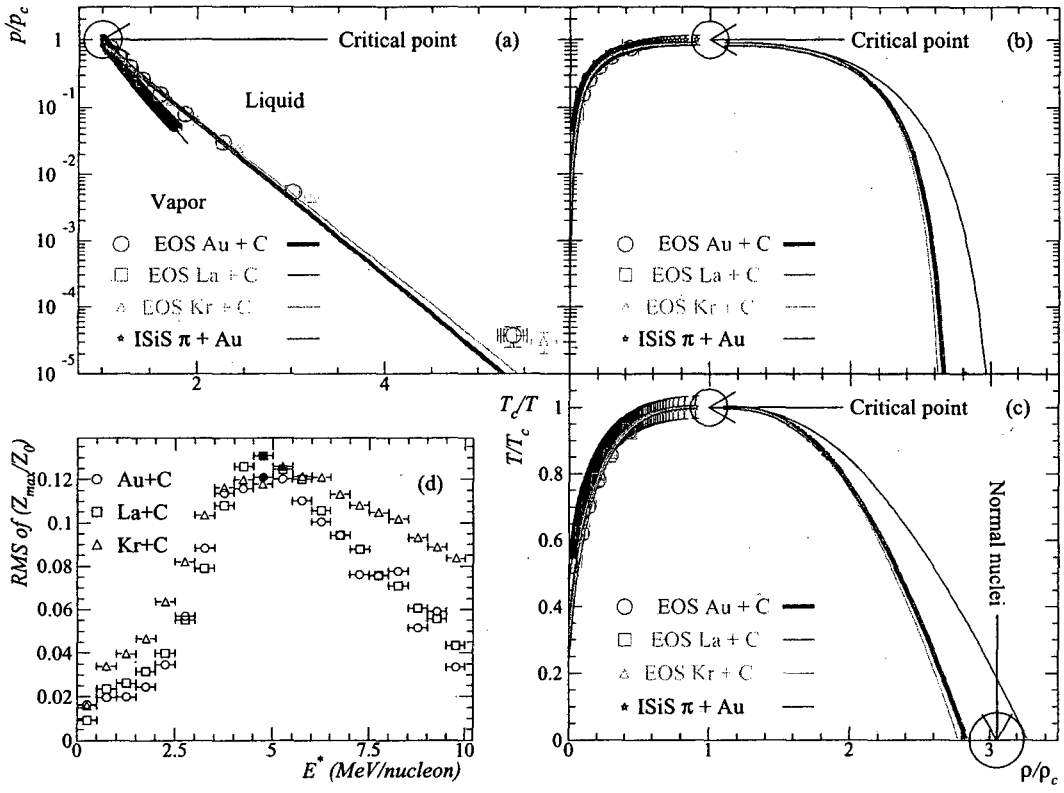

FIGURE 2. (a) The reduced pressure versus inverse reduced temperature, (b) the reduced pressure versus the reduced density and (c) the reduced temperature versus reduced density for the ISiS and EOS systems. (d) The RMS fluctuations of the charge of the largest fragment normalized to the charge of the fragmenting system versus excitation energy for the EOS systems, solid points show E_c^*.

Coulomb factor x is of the same order of magnitude for both experiments. The values of x may indicate more (Au and La) or less (Kr) Coulomb energy. The differences in the amount of secondary decay inferred from the EOS and ISiS results is an open question. The EOS data scaled according to Eq. (2) shows data for all three systems collapsing onto a single line (see Fig. 1), illustrating the common nature of the underlying phenomenon.

THE PHASE DIAGRAM OF FINITE NUCLEAR MATTER

Fisher assumed that a real gas of interacting particles could be treated as an ideal gas of non-interacting droplets; all of the "non-ideality" of the gas is accounted for in the clusterization. Thus the total pressure is found by summing the partial pressures

$$\frac{p}{T} = \sum n_A \tag{5}$$

and the density is simply

$$\rho = \sum n_A A. \tag{6}$$

Accordingly, the reduced pressure is:

$$\frac{p}{p_c} = \frac{T \sum n_A(T)}{T_c \sum n_A(T_c)}. \tag{7}$$

The coexistence line for finite nuclear matter is obtained by using $n_A(T, \Delta\mu = 0, E_{Coul} = 0)$ from Eq. (2) in Eq. (7), transforming Fig. 1 into the familiar form shown in Fig. 2. The EOS gold and lanthanum data show nearly identical results due to their common value of T_c while the krypton data differs due to its different value of T_c. The different slope for the ISiS and EOS data sets is due in part to the differing energy scales. An estimate of the bulk binding energy of nuclear matter was made by recalling the Clausius-Clapeyron equation

$$\frac{dp}{dT} = \frac{\Delta H}{T \Delta V} \tag{8}$$

that leads to

$$\frac{p}{p_c} = \exp\left(\frac{\Delta H}{T_c}\left(1 - \frac{T_c}{T}\right)\right) \qquad (9)$$

which describes several ¤uids up to T_c [22]. The slopes of the coexistence lines and the values of T_c then provide the molar enthalpy of evaporation of the liquid ΔH, shown in Table 2. The energy required to evaporate a fragment, the bulk binding energy, is found from $\Delta H = \Delta E + pV = \Delta E + T$, since $pV = T$ for an ideal gas. Taking into account the average primary fragment size along the coexistence line, ~ 1.5 for ISiS, ~ 1.3 for EOS, gives the ΔE/nucleon shown in Table 2. The value is close to the nuclear bulk energy coef£cient of 16 AMeV. The values of ΔH and ΔE/nucleon from the ISiS data differ form those of the EOS data, due in part to the differing measures of the E^* scale.

The reduced density of the vapor branch of the coexistence curve of £nite nuclear matter is given by:

$$\frac{\rho}{\rho_c} = \frac{\sum A n_A(T)}{\sum A n_A(T_c)}. \qquad (10)$$

This is shown in Fig. 2. It is possible to determine the high density branch as well: empirically, the ρ/ρ_c-T/T_c coexistence curves of several ¤uids can be £t with: [23]

$$\frac{\rho_{l,v}}{\rho_c} = 1 + b_1(1 - \frac{T}{T_c}) \pm b_2(1 - \frac{T}{T_c})^{\beta} \qquad (11)$$

where the parameter b_2 is positive (negative) for the liquid ρ_l (vapor ρ_v) branch. The critical exponent β can be determined via: $\beta = (\tau - 2)/\sigma$ [12]. Table 1 shows the results. Fitting the coexistence curves of the ISiS and EOS data sets with Eq. (11) gives estimates of the full ρ_v branch of the coexistence curve. Changing the sign of b_2 gives the full ρ_l branch of the coexistence curve of £nite nuclear matter. Assuming that normal nuclei exist at the $T = 0$ point of the coexistence curve in Fig. 2, then gives $\rho_c \approx \rho_0/3$.

Dividing the critical pressure by the product of T_c and the critical density gives the critical compressibility factor $C_c^F = p_c/T_c\rho_c$. Table 1 shows the results for the ISiS and EOS data which are in agreement with values of several ¤uids [24]. The pressure at the critical point p_c can be found by using T_c and ρ_c in combination with C_c^F, the results are given in Table 2. This gives the a complete experimental measure of the critical point of £nite nuclear matter (p_c, T_c, ρ_c) that agrees with theoretical calculations [18]. For completeness the p/p_c-ρ/ρ_c projection of the coexistence curve is determined and shown in Fig. 2.

COMPOUND NUCLEUS DECAY AND THE LIQUID TO VAPOR PHASE TRANSITION

The construction of a phase diagram, and in particular of a pressure-temperature diagram for a nuclear system leads us to the inevitable question: What is the meaning of pressure when the nuclear system is facing vacuum? This question has presented itself in many equivalent guises in the literature and in endless discussions. It amounts to asking: a) whether there is a gas phase in equilibrium with a liquid for the reactions in question; and b) whether this gas phase is thermodynamically characterizable. For a compound nucleus the answer is no to a) and yes to b). And this is not contradictory.

To see this point, consider the interface between a liquid and saturated vapor. From the liquid side we can specify with standard theories (e.g. compound nucleus decay rate, the equation for electrons emitted from a hot £lament, etc.) the emission ¤ux of particles from the surface. From the vapor side, we can write down the return ¤ux into the liquid knowing the temperature, pressure/concentration and composition of the vapor. At equilibrium, by de£nition, the vapor to liquid ¤ux matches physically and chemically the liquid to vapor ¤ux. Thus, the saturated vapor acts, so to speak, as a mirror re¤ecting back elastically all the particles emitted by the liquid. This is the only role of the vapor.

If we remove the vapor, the liquid continues emitting particles as if the vapor were still present. Thus, the saturated vapor is completely characterized by the ¤ux from the liquid side, even if the vapor itself is not physically there. So it is that we can unequivocally speak of the phase transition for a glass of water (or a nucleus) evaporating in a dry atmosphere or equivalently in vacuum.

In this light, compound nuclear decay becomes suddenly relevant to the liquid to vapor phase transition. In the past, we have studied the evaporation of complex fragments from well characterized compound nuclei [25]. It should be possible to cast these results in terms of Fisher's scaling. This is done in Fig. 3 for the reaction of Ni+C. As in the previous cases, the scaling is very good and the extracted parameters very close to those of the other systems. From this example we see in these low energy reactions a very interesting source for further characterization of the phase transition, in particular for anchoring the parameters of Fisher's model to the well established $T = 0$ parameters of the liquid drop model.

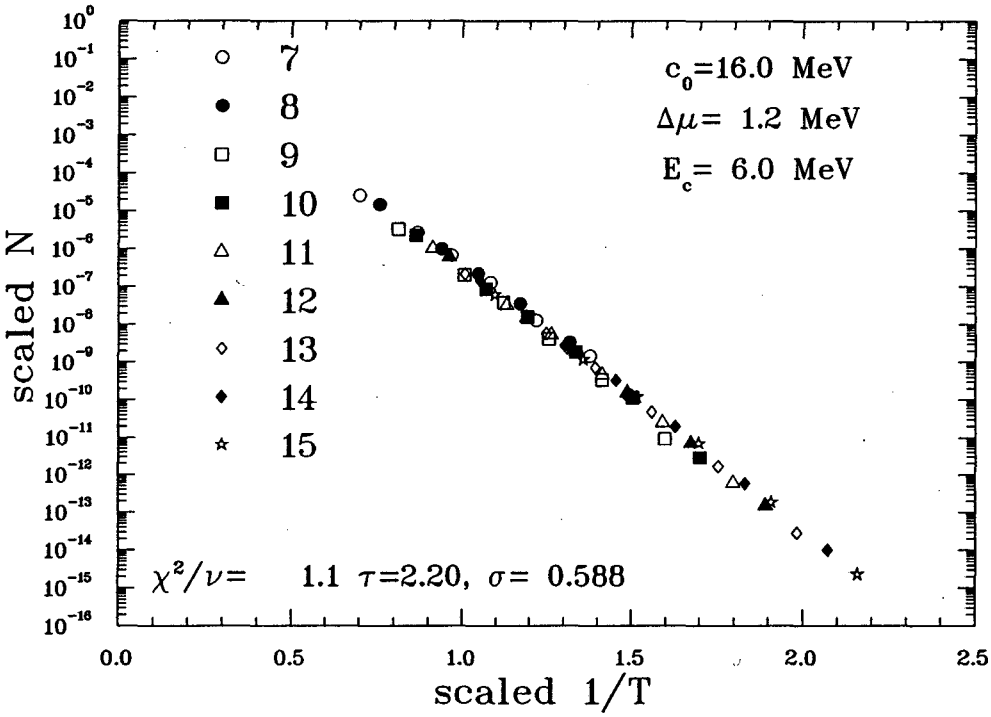

FIGURE 3. Preliminary results for the scaled yield distribution versus the scaled temperature for the Ni+C low energy compound nucleus decay data.

CHEMICAL EQUILIBRIUM VERSUS REACTION RATE DESCRIPTIONS

We now have two competing interpretations of the Fisher scaling. The £rst is the very natural explanation in terms of chemical equilibrium between a gas and a liquid. The second explanation is a reaction rate picture supported by the observation of Fisher scaling of complex fragments emitted from compound nucleus reactions.

Since compound nucleus decay rates (widths Γ) can be calculated using standard theory, then the £rst chance emission yields from a compound nucleus can be used to determine the properties of the nuclear vapor. In other words the £rst chance emission yields can be written

$$\langle n \rangle \propto \Gamma \propto e^{-B/T}. \tag{12}$$

It is noteworthy that the same decay width Γ which controls the £rst chance emission yields also controls the mean emission times (τ) for fragment emission since

$$\Gamma\tau \approx \hbar, \tag{13}$$

and therefore

$$\tau \propto \frac{1}{\Gamma} \propto \frac{1}{\langle n \rangle} \propto e^{B/T}. \tag{14}$$

How do we tell whether the chemical equilibrium picture or the reaction rate picture is the relevant description of the ISiS and EOS data sets? The necessary information has been provided by the ISiS collaboration. They have measured the mean emission time for fragment emission as a function of excitation energy [26, 27]. We have plotted the mean emission times as a function of $1/T$ in Fig. 4. We use the Fermi gas approximation that maps excitation energy to temperature as described previously in this paper. We observe that the lifetimes are well described by a Boltzmann factor, indicating a thermal reaction rate picture as described above.

Furthermore, the lifetimes are consistent with the *same* Boltzmann factor that controls the yields. In Fig. 5, we have plotted the inverse yields of carbon on the same plot as lifetimes determined for $Z = 4 - 9$ as a function of inverse temperature. The Boltzmann factor which describes the yields (the £t to the open points) can be used to describe the lifetimes (solid points). So, not only do the lifetimes appear statistical, they are also governed by the *same* Boltzmann factor as that controlling the yields. Consequently, we are left with a picture very similar to compound nucleus decay which describes the ISiS data up to the critical temperature.

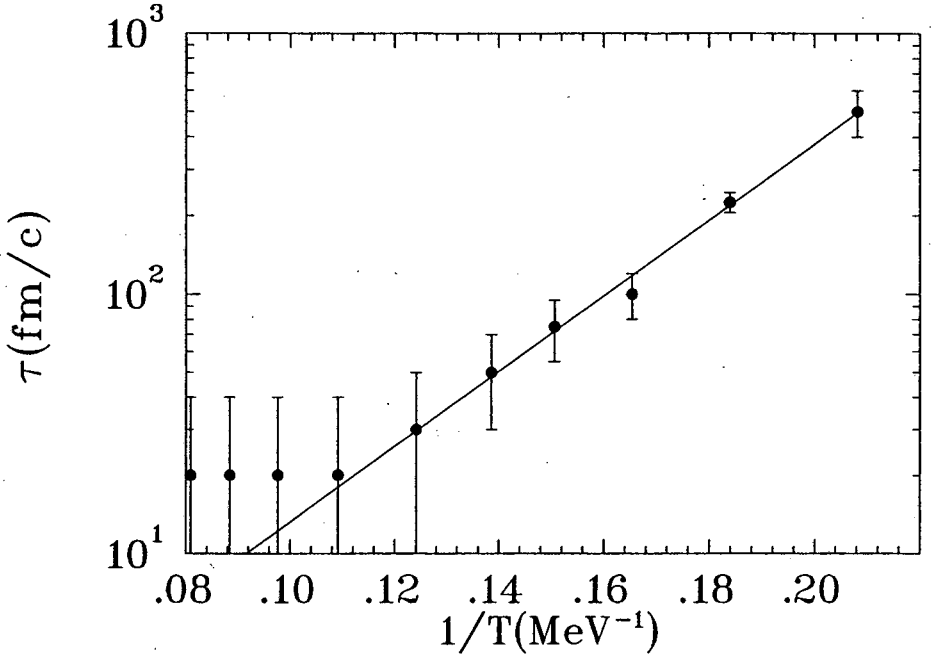

FIGURE 4. The mean emission time in fm/c of fragments with atomic number $Z = 4 - 9$ is plotted versus inverse temperature for the reaction π+Au at 8 GeV/c [26, 27]. The line is a Boltzmann £t to the emission times.

CONCLUSION

In conclusion, the ISiS and EOS data, together with the low energy compound nucleus reaction contain the signature of a liquid to vapor phase transition via their strict adherence to Fisher's model. Through Fisher's scaling of the fragment yield distribution (Fig. 1), the two-phase coexistence line has been determined over a large energy/temperature interval extending up to the critical point. Fisher's formula (Eq. (1)) has been extensively tested and veri£ed for the £rst time for any physical system. The critical exponents τ and σ as well as the critical temperature T_c, the surface energy coef£cient c_0, the enthalpy of evaporation ΔH and the critical compressibility factor C_c^F have been extracted and found to agree with accepted values. Finally, p_c and ρ_c have also been determined, giving the £rst complete experimental determination of the critical point and the full phase diagram of £nite neutral nuclear matter.

Through a direct examination of the mean emission times of the ISiS fragmentation reactions, we infer a sequential emission scenario consistent with complex fragment emission at much lower excitation energies.

This work was supported by the US Department of Energy.

REFERENCES

1. J. E. Finn *et al.*, Phys. Rev. Lett. **49**, 1321 (1982).
2. P. J. Siemens, Nature **305**, 410 (1983).
3. L. G. Moretto *et al.*, Phys. Rep. **287**, 249 (1997).
4. J. B. Elliott *et al.*, Phys. Rev. C **62**, 064603 (2000).
5. J. Pochodzalla *et al.*, Phys. Rev. Lett **75**, 1040 (1995).
6. M. D'Agostino *et al.*, Phys. Lett. B **473**, 219 (2000).
7. J. B. Elliott *et al.*, to be published.
8. J. B. Elliott *et al.*, Phys. Rev. Lett. **88**, 042701 (2002).
9. K. Kwiatkowski *et al.*, NIM A360, 571 (1995).
10. T. Lefort *et al.*, Phys. Rev. Lett **83**, 4033 (1999).
11. J. A. Hauger *et al.*, Phys. Rev. C **62**, 024626 (2000).
12. M. E. Fisher, Physics **3**, 255 (1967).
13. H. Nakanishi and H. E. Stanley, Phys. Rev. B **22**, 2466 (1980).
14. A.H. Raduta *et al.*, Phys. Rev. C **55**, 1344 (1997).
15. K. Hagel *et al.*, Nucl. Phys. **A486**, 429 (1988).
16. M. D'Agostino *et al.*, Nucl. Phys. A **650**, 328
17. M. Kleine Berkenbusch *et al.*, nucl-th/0109062 (2001).
18. J. N. De *et al.*, Phys. Rev. C **59**, R1 (1999).
19. C.M. Mader *et al.*, LBNL-47575.
20. D. Stauffer and A. Aharony, "Introduction to Percolation Theory", second ed. (Taylor and Francis, London, 2001).
21. J. M. Yeomans, "Statistical Mechanics of Phase Transitions", £rst ed. (Clarendon Press, Oxford 1992).
22. E.A. Guggenheim, "Thermodynamics", 4th ed. (North-Holland, 1993).
23. E. A. Guggenheim, J. Chem. Phys., **13**, 253 (1945).
24. C. S. Kiang, Phys. Rev. Lett. **24**, 47 (1970).
25. T. S. Fan, *et ap.*, Nucl. Phys. A **679**, 121 (2000).
26. L. Beaulieu *et al.*, Phys. Rev. Lett. **84**, 5971 (2001).

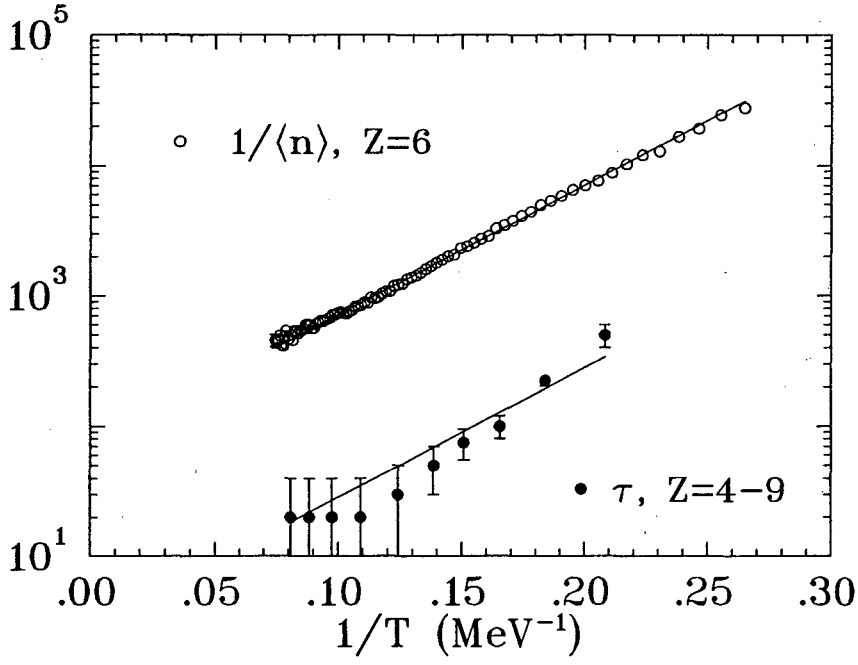

FIGURE 5. The inverse fragment yields (open circles) and emission times (solid circles) are plotted as a function of inverse temperature for the reaction π+Au at 8 GeV/c [26, 27]. The line is a Boltzmann £t to the inverse yields. The same Boltzmann factor is used to describe the emission times.

27. L. Beaulieu *et al.*, Phys. Rev. C **63**, 031302 (2001).

ERNEST ORLANDO LAWRENCE BERKELEY NATIONAL LABORATORY
ONE CYCLOTRON ROAD | BERKELEY, CALIFORNIA 94720

Prepared for the U.S. Department of Energy under Contract No. DE-AC03-76SF00098